The Astrophysical Journal, 589:976–982, 2003 June 1

ASYMPTOTIC GIANT BRANCH AND SUPERGIANT STELLAR DIAMETERS IN THE MID-INFRARED

J. Weiner, D. D. S. Hale, and C. H. Townes
Space Sciences Laboratory and Department of Physics, University of California, Berkeley, CA 94720;
johnw@ssl.berkeley.edu, david@isi.mtwilson.edu, cht@ssl.berkeley.edu
Received 2002 December 20; accepted 2003 February 12

ABSTRACT

The size of the continuum photospheres of α Ori, α Her, R Leo, and χ Cyg have been measured at 11 μm using heterodyne interferometry to accuracies as high as 1%. An assortment of narrow wavelength bands near 11 μm (each having a width $\sim$0.17 cm^{-1}) were used to avoid spectral lines. The resulting apparent diameters for α Ori and α Her are $\sim$30% larger than measured near-infrared sizes, whereas the Mira variables, R Leo and χ Cyg, have 11 μm apparent diameters roughly twice their reported near-infrared sizes. The complexities of interpretation are discussed.

Subject headings: infrared: stars — stars: AGB and post-AGB — stars: individual (χ Cygni, α Herculis, R Leonis, α Orionis) — techniques: interferometric

1. INTRODUCTION

Stars on the asymptotic giant branch (AGB) are characterized by their extremely high luminosities and relatively cool temperatures. Nearing the end of their stellar evolution, AGB stars have a degenerate carbon-oxygen core surrounded by a helium-burning shell and very extended convective zone. Typical photospheric radii are about 500 $R_\odot$. Mira variables are AGB stars that pulsate with a period of about 1 yr and whose visual flux may change by as much as 8 mag.

Because of their large size, AGB stars have surface gravities several orders of magnitude lower than our Sun. This leads to extension of their atmospheres, which is exaggerated in the Mira variables by pulsation. Convective dredge-up causes the heavy products of helium fusion, including significant amounts of carbon and oxygen, to be dispersed throughout the outer layers of the star. In the cool stellar atmosphere, densities are sufficient for the formation of di- and polyatomic molecules including CO, TiO, SiO, and H_2O. At several stellar radii, temperatures fall enough for metal-oxide or carbon dust grains to condense. The forest of molecular spectral lines combined with absorption and scattering from the dust leads to atmospheric opacities that depend sensitively on wavelength and temperature. These effects can lead to exotic intensity distributions not at all like the nearly uniform intensity stellar disk exhibited by our Sun. They can also substantially affect measurements of stellar angular diameters (Hofmann & Scholz 1998; Jacob et al. 2000).

A sample of published apparent stellar diameters in the visible and near-infrared, listed in Table 1, exhibits the large variations with wavelength indicated above. Table 1 lists the wavelength, variability phase (for the Mira variables), angular radius, implied linear radius (assuming *Hipparcos* parallaxes with no error contribution), observation method, instrument, and reference for apparent size measurements of α Ori, α Her, R Leo, and χ Cyg, found to have been published since 1980. Discrepancies between measurements at different wavelengths as large as 44% in α Ori and over 100% for the Mira variables R Leo and χ Cyg are seen. In some cases, models relating diameter measurements in adjacent bands (Quirrenbach et al. 1993) and at a variety of wavelengths (Hofmann & Scholz 1998; Hofmann, Scholz, & Wood 1998) have been constructed, but to date, no complete model that accounts for measured apparent diameters at all wavelengths including the mid-infrared has been published. The importance of interpreting apparent size measurements properly and avoiding extraphotospheric opacity contributions to obtain an unbiased stellar diameter is clear.

In addition to wavelength-dependent size fluctuations, there are other complications preventing a direct identification of apparent size with stellar radius. Limb darkening, important at visible and near-infrared wavelengths for stars having a steep photospheric temperature gradient, systematically reduces the apparent stellar size. Hot spots on the stellar surface, capable of lowering apparent sizes on the order of 15%,[1] are predicted to exist on AGBs (Schwarzschild 1975), and asymmetric hot spots varying on a weekly timescale and contributing more than 20% of the 700 nm flux have been observed on α Ori (Wilson, Dhillon, & Haniff 1997). Furthermore, periodic size variations are predicted to occur in Mira variables (Ya'ari & Tuchman 1999; Bessel, Scholz, & Wood 1996) and have been observed in R Leo (Burns et al. 1998) and χ Cyg (Young et al. 1999).

The Infrared Spatial Interferometer (ISI) is a heterodyne detection interferometer utilizing CO_2 laser local oscillators and operating at various wavelengths between 9.5 and 11.5 μm. It is located at Mount Wilson Observatory, a site chosen for its excellent seeing. For these observations, the ISI consisted of two 1.65 m telescopes separated by various baselines up to 56 m. A more detailed description of the instrument can be found in Hale et al. (2000). The ISI is particularly well suited for measuring AGB stellar diameters because of its wavelength and narrow bandpass. In the mid-infrared, intensity is much less sensitive to temperature changes than at shorter wavelengths. Consequently, any hot spots present on the stellar photosphere would bias ISI diameter measurements substantially less than in the visible or near-IR. Also, limb darkening effects are expected to be less in the mid-infrared than at shorter wavelengths (Manduca 1979). The ISI is able to avoid spectral line contamination by selecting a bandpass that does not contain strong molecular transitions from the $\sim$100 available

[1] See Weiner (2002) for a discussion of this estimate.

TABLE 1

SELECTED PUBLISHED VISIBLE AND NEAR-INFRARED DIAMETERS OF α ORI, α HER, R LEO, AND χ CYG

Star	λ (μm)	Phase	ϕ (mas)	Radius[a] ($R_\odot$)	Method[b]	Instrument	Reference
α Ori	0.370		52 ± 6	733 ± 85	AM	KPNO 4 m Telescope	1
	0.410		51 ± 2	719 ± 28	AM	KPNO 4 m Telescope	1
	0.520		50 ± 1	705 ± 14	AM	KPNO 4 m Telescope	1
	0.546		57 ± 2	804 ± 28	AM	Herschel Telescope	2
	0.550		48 ± 1	677 ± 14	AM	KPNO 4 m Telescope	1
	0.633		55 ± 1	776 ± 14	AM	Herschel Telescope	2
	0.650		58 ± 1	818 ± 14	AM	KPNO 4 m Telescope	1
	0.656		44 ± 1	620 ± 14	AM	KPNO 4 m Telescope	1
	0.700		49 ± 3	691 ± 42	AM	Herschel Telescope	2
	0.710		54 ± 2	762 ± 28	AM	Herschel Telescope	2
	0.800		49.4 ± 0.5	697 ± 7	I	Mark III	3
	0.830		51.1 ± 1.5	721 ± 21	I	COAST	4
	0.850		46 ± 1	649 ± 14	AM	KPNO 4 m Telescope	1
	0.854		43 ± 1	607 ± 14	AM	KPNO 4 m Telescope	1
	1.09		42 ± 2[c]	592 ± 25	AM	Keck Telescope	5
	1.28		42 ± 2[c]	592 ± 25	AM	Keck Telescope	5
	1.64		41.5 ± 2[c]	585 ± 25	AM	Keck Telescope	5
	2.12		42 ± 2[c]	592 ± 25	AM	Keck Telescope	5
	2.2		44.2 ± 0.2	623 ± 2.8	I	Michelson Array	6
	3.09		48 ± 2[c]	677 ± 25	AM	Keck Telescope	5
	3.75		40.2 ± 0.2	567 ± 2.8	I	IOTA	7
	Several		41.0 ± 0.8	578 ± 11	P	Several	8
α Her	2.2		32.2 ± 0.8	403 ± 10	I	Michelson Array	9
	2.2		30.90 ± 0.02	387.13 ± 0.25	I	IOTA	7
	3.75		32.8 ± 0.7	411 ± 8.8	I	IOTA	7
R Leo	0.650	0.24	67 ± 5	731 ± 55	LO	Cape, Royal Obs.	10
	0.700	0.88	64.2 ± 5.7	700 ± 62	AM	Herschel Telescope	11
	0.710	0.88	67.9 ± 7.0	740 ± 76	AM	Herschel Telescope	11
	0.830	0.05–0.60	36–52	414–556	I	COAST	4
	0.830	0.39–0.60	48–51	523–556	AM	Herschel Telescope	4
	0.833	0.27	44.9 ± 2.0	490 ± 22	AM	Herschel Telescope	11
	0.902	0.27	43.3 ± 2.0	472 ± 22	AM	Herschel Telescope	11
	0.940	0.05–0.60	36–52	393–567	I	COAST	4
	0.940	0.39–0.60	47–50	512–545	AM	Herschel Telescope	4
	2.16	0.2	33 ± 1.3	360 ± 14	LO	TIRGO IR Tel.	12
	2.2	0.24	28.18 ± 0.05	307.3 ± 0.5	I	IOTA	13
	2.2	0.28	30.68 ± 0.05	334.5 ± 0.5	I	IOTA	13
	3.5	0.64	50	545	LO	Hale Observatory	10
	3.75	0.3	44.5 ± 0.2	485 ± 2.2	I	IOTA	7
	3.79	0.81	36.02 ± 0.52	393 ± 5.7	I	IOTA	14
	3.79	0.62	39.08 ± 3.3	426 ± 36	I	IOTA	14
	4.8	0.64	50	545	LO	Hale Observatory	10
χ Cyg	0.700	0.14–0.35	34–44	388–502	AM	Herschel Telescope	11
	0.710	0.14	41 ± 4	468 ± 46	AM	Herschel Telescope	11
	0.833	0.32	33 ± 4	377 ± 46	AM	Herschel Telescope	11
	0.902	0.32	33 ± 2	377 ± 23	AM	Herschel Telescope	11
	0.905	0.73–1.00	24.7–33.6[d]	282–383[d]	I	COAST	15
	1.024	0.73–1.00	22.3–30.7[d]	255–350[d]	I	COAST	15
	1.290	0.73–1.00	19.5–22.4[d]	223–256[d]	I	COAST	15
	2.16	0.38	23.24 ± 0.08	265.3 ± 0.9	I	IOTA	14
	3.79	0.81	30.40 ± 7.28	347 ± 83	I	IOTA	14

[a] Distances of 131, 116, 101, and 106 pc were assumed for α Ori, α Her, R Leo, and χ Cyg, respectively. The errors quoted are from the error in the angular diameter only and do not include uncertainty in the adopted distance.

[b] AM: aperture masking; I: interferometry; P: infrared photometry; LO: lunar occultation.

[c] Estimated from plot in Tuthill, Monnier, & Danchi 1999 and error quoted in Weiner et al. 2000 using a similar method.

[d] Implied uniform-disk diameter. The reference listed a Gaussian FWHM, which was assumed to be a factor of 1.61 times smaller.

REFERENCES.—(1) Cheng et al. 1986; (2) Wilson et al. 1992; (3) Mozurkewich 1991; (4) Burns et al. 1997; (5) Tuthill et al. 1999; (6) Dyck et al. 1992; (7) Mennesson et al. 2000; (8) Morgan, Wasatonic, & Guinan 1997; (9) Benson et al. 1991; (10) White & Feierman 1987; (11) Haniff, Scholz, & Tuthill 1995; (12) di Giacomo et al. 1991; (13) Perrin et al. 1999; (14) Mennesson et al. 2002; (15) Young et al. 1999.

narrow (0.17 cm^{-1}) bandpasses. Finally, the spatial frequency coverage of the ISI allows for the important separation of dust shell intensities from those of the stellar disk.

2. OBSERVATIONS

The 11 μm stellar diameters are obtained from ISI raw visibility data (visibility squared, V_i^2, with error, σ_i, as a function of spatial frequency, x_i) by fitting it with the visibility curve of a uniform disk (UD) of radius, r. The presence of an extended dust shell is allowed for with a second parameter, A, which lowers the visibilities by an amount equal to the fraction of light coming from the dust shell. Specifically, the best-fitting radius is taken to be the minimum of $\chi^2(r, A)$,

$$\chi^2(r, A) = \frac{\sum_{i=1}^{N} \left\{ [V(x_i, r, A)]^2 - V_i^2 \right\}^2}{\sigma^2_{V_i^2}} , \qquad (1)$$

where the visibility function of the uniform disk, $V(x, r, A)$, is given by

$$V(x, r, A) = \frac{2AJ_1(2\pi rx)}{2\pi rx} . \qquad (2)$$

Here, J_1 is the Bessel function of order unity, and the dust shell is assumed to be fully resolved at the spatial frequencies fit. The validity of this assumption will be further discussed for each star separately. It should be noted that any error in the calibration of the visibility will be absorbed into the parameter A and will not affect the fitted diameter (only the estimate of the fraction of the flux coming from the dust). The error in the best-fit radius was estimated as one-half the full width (in r) of the region of the A-r plane in which the χ^2, normalized such that its minimum, $N - 2$, is increased by no more than unity from its minimum

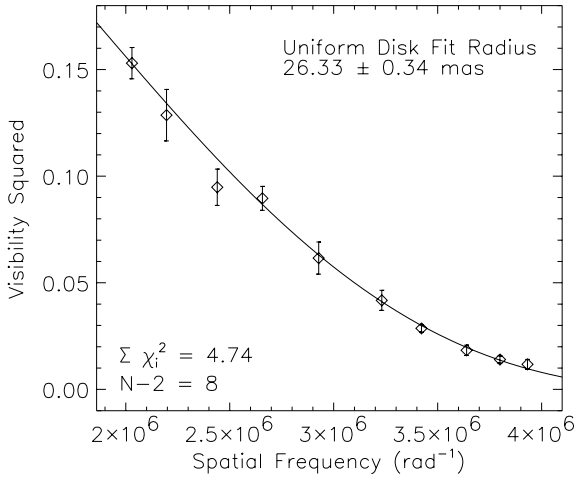

FIG. 1.—ISI data for α Ori from 2001 December 19. The best-fitting uniform disk has a radius of 26.33 mas with 55.6% of the 11 μm flux coming from the stellar disk.

(Bevington 1969). Figure 1 contains an example of α Ori visibility data from 2001 December 19 and its best-fitting uniform-disk curve. Often, as in this case, a single night of observations yields enough data to be reasonably fitted with a uniform disk. For weaker stars, or in worse seeing conditions, we may combine several nights together before fitting. There is rarely a case when data spanning more than a week are fitted together since changes in the star with time or stellar phase are to be expected.

All ISI diameter measurements for α Ori, α Her, R Leo, and χ Cyg between 1999 and 2001 are listed in Table 2. For consistency, and to minimize the effect of any unresolved dust, only spatial frequencies greater than 1.75×10^6 rad^{-1} (which resolve structures larger than 0.″06) were used in the fits. Each observation was made in a bandpass centered at the wavelength listed, λ, and having a full width of $\sim$2 nm

TABLE 2
INFRARED SPATIAL INTERFEROMETER DIAMETER MEASUREMENTS OF α ORI, α HER, R LEO, AND χ CYG MADE IN 1999–2001

Star	Dates	Phase	λ (μm)	ϕ (mas)	Radius[a] ($R_\odot$)
α Ori	1999 Nov 10–19		11.149	54.94 ± 0.30	774.9 ± 4.2
	2000 Nov 1, 8		11.149	53.42 ± 0.62	753.5 ± 8.7
	2000 Nov 28, 29		11.149	55.78 ± 0.92	786.8 ± 13.0
	2000 Dec 21		11.149	54.80 ± 1.00	773.0 ± 14.1
	2001 Aug 16–24		11.149	53.38 ± 0.64	752.9 ± 9.0
	2001 Sep 27, 28		11.149	53.28 ± 0.40	751.5 ± 5.6
	2001 Oct 4		11.149	52.56 ± 0.78	741.4 ± 11.0
	2001 Oct 11–19		11.149	53.10 ± 0.52	749.0 ± 7.3
	2001 Oct 25, 26		11.086	54.14 ± 0.52	763.6 ± 7.3
	2001 Nov 9, 16		11.171	54.20 ± 0.46	764.5 ± 6.5
	2001 Dec 19		11.149	52.66 ± 0.68	742.8 ± 9.6
α Her	2001 Jul 18–31		11.149	39.32 ± 1.04	496.1 ± 13.1
R Leo.....	1999 Oct 28	0.43	11.149	55.30 ± 5.00	603.0 ± 54.5
	2001 Oct 19; Nov 2–8	0.77	11.149	62.62 ± 1.14	682.8 ± 12.4
	2001 Nov 9, 16	0.81	11.171	64.24 ± 1.12	700.5 ± 12.2
χ Cyg	2001 Jul 27, 30; Aug 23	0.51	11.149	39.38 ± 4.02	449.4 ± 45.9

[a] Distances of 131, 116, 101, and 106 pc were assumed for α Ori, α Her, R Leo, and χ Cyg, respectively. The errors quoted are from the error in the angular diameter only and do not include uncertainty in the adopted distance.

(or 0.17 cm^{-1} in wavenumber). High-resolution spectra[2] of each star around the bandpasses used are shown in Figure 2. The flux is plotted as a function of wavenumber with dashed vertical lines marking the approximate edges of the ISI bandpass as it would appear on the date shown.[3] Vertical bars mark H_2O transitions (with line strength[4] given by the right axis). These H_2O spectral lines are evident in all of the stars except χ Cyg. (There are more spectra not shown here that further support this conclusion.)

2.1. α *Ori*

The M1/M2 supergiant α Ori is a semiregular variable and is thought to have a mass on the order of 10 $M_\odot$. The 11 μm size of α Ori was measured to be about 30% larger than the smallest of the near-IR sizes. Each of the three bandpasses used to observe α Ori do not contain strong H_2O transitions, nor are any spectral lines evident within their bandpasses in the spectra shown in Figure 2. The dust shell of α Ori, modeled at 11 μm by Danchi et al. (1994), exists only at radii greater than $40R_*$ and is fully resolved at the spatial frequencies measured here. This result comes largely from measurements in 1989. Further measurements made about 3 yr later indicate additional emission of a small amount of dust with an inner radius of approximately $4R_*$ (Bester et al. 1996). This small amount of dust should have expanded to at least twice this distance from the star when the present measurements were made. Negligible (<0.1%) error is introduced to the diameter measurement by such a dust shell (Weiner 2002). The effect of limb darkening is capable of lowering the apparent diameter and was confirmed in α Ori at 830 nm (Burns et al. 1997). However, the stellar intensity profile tends to become more uniform disk–like with increasing wavelength and at 11 μm should be quite flat (Manduca 1979). Additionally, hot spots or other temperature inhomogeneities, capable of lowering apparent diameters on the order of 15% in the near-infrared (Weiner 2002), are much less pronounced at 11 μm.

The 11 μm monochromatic radius (radius at which $\tau_{11\ \mu m} = 1$) can be estimated in terms of the Rosseland radius by comparing the Rosseland opacity with the 11 μm opacity in the stellar photosphere. The Rosseland opacity was calculated for a gas of solar abundance at a variety of densities and temperatures by Alexander & Ferguson (1994). The 11.149 μm opacity of solar abundance gas was calculated by solving for the ionization state of the gas (including elements up to $Z = 28$) and the dissociation of H_2 assuming local thermodynamic equilibrium and summing the contributions of H^-_{ff}, $H^-_{2\,ff}$, He^-_{ff}, Z_{ff}, Thomson scattering, and Rayleigh scattering, where Z_{ff} refers to free-free processes of every singly ionized atom up to $Z = 28 (Z^+ + e^- \Leftrightarrow Z^+ + e^- + \gamma)$. This calculation is described in detail in Weiner (2002). The resulting ratio of 11.149 μm opacity to Rosseland opacity is plotted in Figure 3 as a function of density for several values of

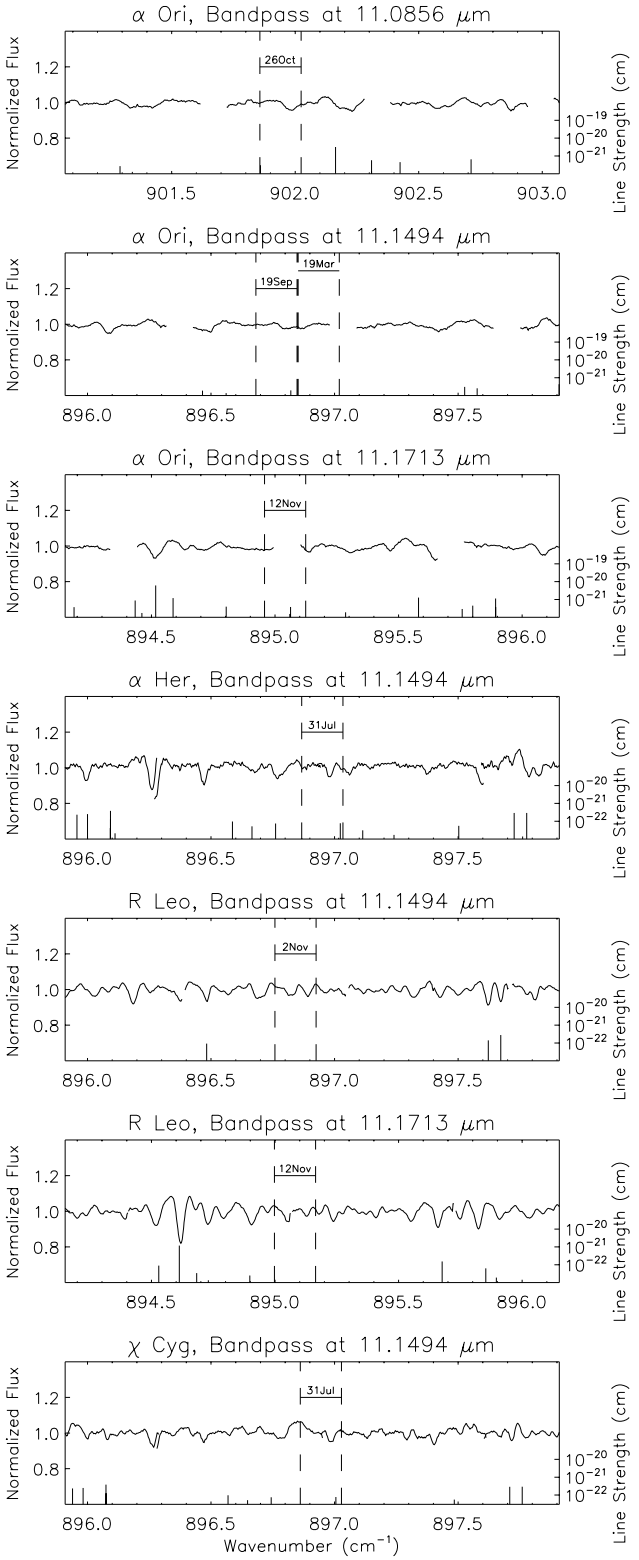

FIG. 2.—Spectra of α Ori, α Her, R Leo, and χ Cyg near the bandpasses that were used. Dashed vertical lines mark the approximate edges of the bandpass at the date shown. Vertical bars mark prominent H_2O transitions with line strength given by the right axis.

[2] The spectra were recorded at the Infrared Telescope Facility telescope using the TEXES instrument. The observations were carried out by John Lacy and Matt Richter, and a description of the instrument can be found in Lacy et al. (2002).

[3] The spectra are Doppler-shifted by Earth's motion around the Sun. Since there were several α Ori observations at 11.149 μm, only the extrema of Earth's motion were shown here. The bandpass at all other dates lies between those shown.

[4] Line strengths were calculated from the HITRAN/HITEMP database (Rothman et al. 1992) assuming temperatures of 1750, 1500, 1000, and 1500 K and velocities with respect to the Earth of 39, −28, 7, and −22 km s^{-1} for α Ori, α Her, R Leo, and χ Cyg, respectively.

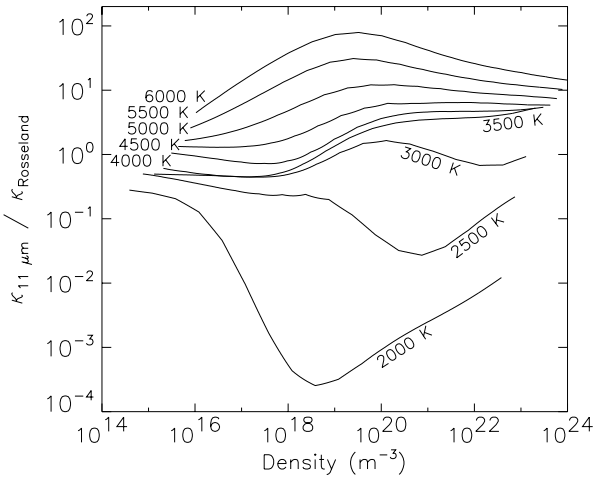

FIG. 3.—Ratio of 11.149 μm opacity to Rosseland opacity as a function of atomic density for several values of temperature.

temperature. At low temperatures, the Rosseland opacity is larger than the 11 μm opacity and is dominated by molecular transitions while the 11 μm opacity is limited by the availability of the few free electrons donated from easily ionized metals such as K, Na, Al, and Ca. As the temperature increases, the molecules dissociate and the Rosseland opacity decreases while the 11 μm opacity increases because of increasing metallic ionization. By 6000 K, ionized hydrogen dominates both opacities and the λ^2 wavelength dependence causes the 11 μm opacity to be larger than the visible and near-IR–dominated Rosseland opacity. At AGB photospheric temperatures ($\sim$3000 K), the Rosseland opacity is comparable to the 11.149 μm opacity (over a large range of densities). Even at temperatures as high as 5000 K, 11 μm opacity is no more than 1 order of magnitude larger than Rosseland opacity. Because of the rapid decrease in density with radius near the stellar surface, it is expected that the 11 μm photosphere will be *near* the Rosseland radius.

A more quantitative estimate of the 11 μm photosphere can be made by considering the density stratification near the stellar surface. Hydrostatic equilibrium will hold at the stellar surface if both radiation pressure and dynamic effects are negligible. The former condition, approximating the radiation pressure by a frequency independent term, is

$$\frac{L_* \kappa_{\rm Rosseland}}{4\pi r^2 c} \ll \frac{GM_* \rho}{r^2} \ . \tag{3}$$

Taking $L_* = 57{,}000\ L_\odot$, $T = 3000$ K, $M_* = 10\ M_\odot$, $\rho = n\overline{m}$, and $\overline{m} = 1.26\ {\rm g}/N_{\rm A}$, where n is the density of atoms and $N_{\rm A}$ is Avogadro's number, the term on the left is several orders of magnitude smaller than the term on the right for densities between 10^{16} and 10^{22} m^{-3}. Hence, the radiation pressure is negligible, and we can assume that hydrostatic equilibrium holds so that the density at the stellar surface falls off like $e^{-\overline{m}gr/kT}$, where $T = 3000$ K and

$$g = \frac{GM_*}{R_*^2} \approx \frac{G \times 10\ M_\odot}{(750\ R_\odot)^2} = 0.491\ {\rm cm\ s^{-2}} \ . \tag{4}$$

Then, the density is lowered by 1 order of magnitude in a distance, Δr, given by

$$\log(10) = \frac{\overline{m} g\, \Delta r}{kT}$$
$$\Delta r = \frac{2.3kT}{\overline{m}g} = 9.29 \times 10^9\ {\rm m} = 13.3\ R_\odot = 0.018 R_* \ . \tag{5}$$

Hence, a difference in opacity of 1 order of magnitude will affect the radius at which $\tau = 1$ by only $\sim$2%. Since the 11.149 μm opacity was found to be within an order of magnitude of the Rosseland opacity for relevant temperatures and densities, it can be concluded that the measured apparent 11 μm diameters of α Ori differ by no more than a few percent from its Rosseland diameter, provided that the photosphere of α Ori is not *extremely* nonhydrostatic and that dynamic effects do not dominate the density stratification.

Figure 4 plots the size measurements of α Ori listed in Tables 1 and 2. The measurements at wavelengths shorter than 900 nm exhibit large variations presumably because of molecular line blanketing. The near-IR measurements are smaller and more consistent than the shorter wavelength data and show a slight increase in size toward longer wavelengths. The 11 μm apparent size of α Ori is roughly 30% larger than these. The synthetic uniform-disk sizes of the X320 model from Hofmann & Scholz (1998) are also plotted in Figure 4. Although this model refers to a 1 $M_\odot$ star with an effective temperature of 3200 K and a Rosseland radius of 326 $R_\odot$, it qualitatively exhibits some of the same fluctuations as the α Ori data, even though α Ori is believed to be much more massive. However, this model predicts the near-IR uniform-disk radii to be close to the Rosseland radius, in contradiction with the argument above that held that the 11 μm apparent size should be close to the Rosseland size. All of this would tend to imply that the density stratification of α Ori may be very nonhydrostatic near its photosphere and/or that other effects such as hot spots are responsible for reducing the near-IR apparent sizes.

Some small but significant variations with time were observed in the apparent size of α Ori. Nonperiodic fluctuations in the apparent diameter as large as $\pm$2% from average were observed, in some cases, on a weekly timescale. Such

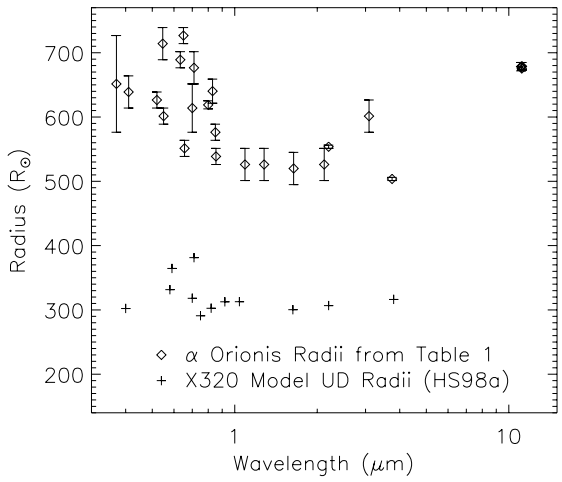

FIG. 4.—Uniform-disk (UD) radius measurements of α Ori from Table 1 and UD radii from the X320 model of Hofmann & Scholz (1998). X320 is a solar composition, 1 $M_\odot$, $10^4\ L_\odot$ model with $T_{\rm eff} = 3200$ K.

deviations may be caused by changing surface features, such as hot spots, rather than actual size changes. No significant size variation was observed between the near-simultaneous measurements at each of the three wavelengths 11.149, 11.086, and 11.171 μm.

2.2. α *Her*

α Her is an M5 supergiant and semiregular variable. As for α Ori, the 11 μm diameter of α Her is about 30% larger than the smallest of the near-infrared diameters listed in Table 1. The spectrum of α Her, shown in Figure 2, does not appear to contain any substantial spectral lines within the bandpass at 11.149 μm, and the dust shell surrounding α Her modeled in Danchi et al. (1994) is located beyond 18 R_*.[5] It is concluded that neither spectral lines nor dust is predicted to significantly alter the diameter measurements (see calculations described in Weiner 2002). Additionally, as for α Ori, limb darkening and hot spots are reduced at 11 μm compared with shorter wavelengths. Repeating the calculation made for α Ori but taking $M_* = 2\ M_\odot$ (Woolf 1963) and $R_* = 500\ R_\odot$, we get $g = 0.220$ cm s^{-2}, implying that the distance over which gas density changes by an order of magnitude, Δr, is $0.060R_*$. So, it is expected that the 11.149 μm apparent size of α Her is within 6% of its Rosseland diameter.

2.3. *R Leo,* χ *Cyg*

R Leo and χ Cyg are Mira variables of spectral types M6–M9 and S6, respectively. Both stars were measured to have an apparent size at 11 μm about *twice* as large as their smallest near-infrared sizes. Some timelike variation in the diameter of R Leo was observed between 1999 and 2001, and no change was seen between 11.149 and 11.171 μm. From Figure 2, the spectra of these stars appear not to contain any strong spectral lines within the bandpasses, indicating that molecular line contamination of the 11 μm diameters is minimal.

The atmospheres of Mira variables are dominated by the periodic passage of shocks that significantly extend the atmosphere and induce the formation of dust much closer to the stellar photosphere ($\sim 2R_*$) than in nonpulsating giant stars (Höfner et al. 1998). The dust shells of R Leo and χ Cyg were characterized by Danchi et al. (1994), and their inner radii were found to be at $\sim 2R_*$ and $15R_*$, respectively. A more recent measurement of the dust surrounding χ Cyg gives an inner radius of $\sim 4R_*$ (S. Tevousjan 2002, private communication). These dust shells may not be fully resolved at the spatial frequencies recorded. It is estimated that, depending on the exact radius of formation of the dust, the uniform-disk diameter will be biased by $\pm 3\%$ for R Leo and $\pm 1\%$ for χ Cyg (Weiner 2002). At any rate, the sizes measured determine the 11 μm continuum photosphere to within a few percent and are much larger than near-IR measured sizes.

The location of the 11 μm continuum photosphere predicted by the Mira models of Bessel et al. (1996) has been discussed in Weiner, Hale, & Townes (2003). The 11 μm opacity was calculated assuming LTE for the density and temperature structure given in the model. Then, the intensity profile was constructed by integrating a blackbody source function over the opacity distribution. Finally, a uniform disk was fitted to the visibility function corresponding to the calculated intensity profile. The radius at which the 11 μm optical depth reached unity was calculated to be almost exactly equal to the Rosseland radius. The 11 μm apparent size (resulting from the uniform-disk fit) was found to be 3.9% greater than the Rosseland diameter (Weiner et al. 2003). Although simplifications made in the calculation, such as the assumption of LTE, may affect these numbers somewhat, these are minor compared with the large variations discussed below.

Figure 5 plots the size measurements of R Leo listed in Tables 1 and 2 as well as the predicted uniform-disk radii of the Mira models Z34890 and Z35280 from Hofmann et al. (1998). The same patterns evident in Figure 4 appear to be present in Figure 5 although much more extreme. The 700 nm size is roughly twice the 2 μm size, and the apparent size appears to increase with wavelengths longer than 2 μm. The two models shown refer to a 1 $M_\odot$ Mira variable with a period of 334 days at maximum (Z34890) and minimum (Z35280). The Rosseland radius at maximum and minimum is predicted to be 260 and 210 $R_\odot$, respectively. As for α Ori, the near-IR sizes are predicted from the above models to be close to the Rosseland size. However, the 11 μm size (which is almost twice the 2 μm measurements) was noted above to be only 3.9% greater than the Rosseland diameter according to model calculations. Furthermore, the two Mira models predict only a slight increase in size between the 2.2 and 3.8 μm bands, whereas an increase of more than 30% was observed. Finally, the absolute values of the measured sizes are larger than the predicted uniform-disk radii at all wavelengths by at least 35%. All of this tends to imply that the Mira models considered are not extended enough.

The existence of a diffuse continuum halo, such as postulated by Mennesson et al. (2002) to exist around R Leo, could produce the large observed increase in apparent size between the near-IR and 11 μm. However, none of the dynamic Mira models published (Bowen 1988; Bessel et al. 1996; Höfner et al. 1998) predict densities sufficient to contribute significant continuum optical depth at radii beyond the photosphere. Furthermore, the data presented in Mennesson et al. (2002) do not demand this interpretation.

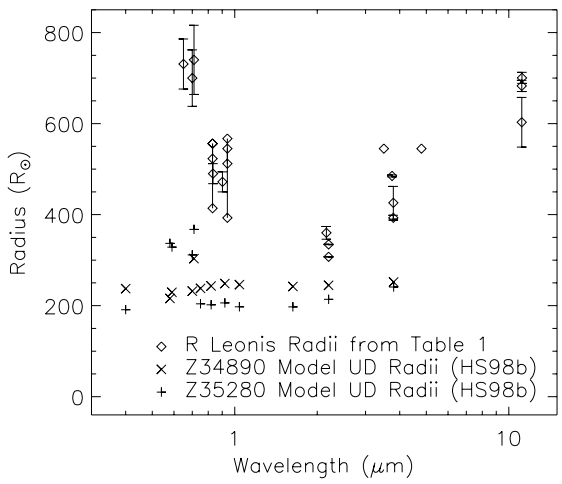

FIG. 5.—Uniform-disk radius measurements of R Leo from Table 1 and UD radii from the Z34890 and Z35280 models of Hofmann et al. (1998). These models describe a 1 $M_\odot$ fundamental mode Mira variable with a period of 334 days at maximum and minimum, respectively.

[5] There is evidence that the dust shell present in 1992 has evolved. (S. Tevousjan et al. 2003, in preparation).

A $28\% \pm 11\%$ increase in the diameter of R Leo was measured between the K' and L' bands, but the measurements occurred almost at opposite phase. Also, no dust shell was taken into account whereas the dust shell measured at 11 μm by Danchi et al. (1994) around R Leo would lower the 2.16 and 3.79 μm visibilities by 15%–20% relative to a uniform disk, thus affecting the measured diameter at these wavelengths.

3. CONCLUSIONS

Heterodyne interferometry has been used at 11 μm to measure the size of several stars with a precision as high as 1%. Dust and spectral lines have negligible effect on the 11 μm apparent diameters of α Ori and α Her, although R Leo and χ Cyg acquire small errors of $\pm 3\%$ and $\pm 1\%$, respectively, because of their dust shells. In addition, the 11 μm intensity distribution will be more uniform than at shorter wavelengths due to the less sensitive dependence of intensity on temperature. Thus, hot spots evident at visible and near-IR wavelengths are much less evident at 11 μm. It is concluded that the measured diameters accurately characterize the 11 μm continuum photosphere.

The 11 μm size of each star is larger than near-infrared diameters: the supergiants by about 30%, and the Mira variables by about 100%. Currently, no published models predict apparent size in the mid-infrared. However, the 11 μm continuum photosphere can be shown to be close to the Rosseland diameter for the case in which the stellar surface is in hydrostatic equilibrium or that in which the densities and temperatures from the Mira model of Bessel et al. (1996) are assumed. This would imply that the near-IR apparent sizes are much smaller than the Rosseland diameter (since they are substantially smaller than the ISI 11 μm sizes). We can conclude that either the smaller sizes measured in the near-infrared are strongly biased due to hot spots or other very strong surface intensity nonuniformity or that the simple hydrostatic assumptions and Mira model considered here give too steep a density gradient at the stellar surface and that higher densities are needed at large radii to account for the observations.

This work was supported in part by the National Science Foundation (AST 97-31625) and the Office of Naval Research (N00014-89-J-1583). We are grateful to Matt Richter and John Lacy for their privately supplied mid-IR spectrum of α Ori, α Her, R Leo, and χ Cyg, and also to Jason Aufdenberg and John Monnier for their help and advice.

REFERENCES

Alexander, D. R., & Ferguson, J. W. 1994, ApJ, 437, 879
Benson, J. A., Dyck, H. M., Mason, W. L., Howell, R. R., Ridgway, S. T., & Dixon, D. J. 1991, AJ, 102, 2091
Bessell, M. S., Scholz, M., & Wood, P. R. 1996, A&A, 307, 481
Bester, M., Danchi, W. C., Hale, D., Townes, C. H., Degiacomi, C. G., Mékarnia, D., & Geballe, T. R. 1996, ApJ, 463, 336
Bevington, P. R. 1969, Data Reduction and Error Analysis for the Physical Sciences (New York: McGraw-Hill)
Bowen, G. H. 1988, ApJ, 329, 299
Burns, D., et al. 1997, MNRAS, 290, L11
———. 1998, MNRAS, 297, 462
Cheng, A. Y. S., Hege, E. K., Hubbard, E. N., Goldberg, L., Strittmatter, P. A., & Cocke, W. J. 1986, ApJ, 309, 737
Danchi, W. C., Bester, M., Degiacomi, C. G., Greenhill, L. J., & Townes, C. H. 1994, AJ, 107, 1469
di Giacomo, A., Lisi, F., Calamai, G., & Richichi, A. 1991, A&A, 249, 397
Dyck, H. M., Benson, J. A., Ridgway, S. T., & Dixon, D. J. 1992, AJ, 104, 1982
Hale, D. D. S., et al. 2000, ApJ, 537, 998
Haniff, C. A., Scholz, M., & Tuthill, P. G. 1995, MNRAS, 276, 640
Hofmann, K.-H., & Scholz, M. 1998, A&A, 335, 637
Hofmann, K.-H., Scholz, M., & Wood, P. R. 1998, A&A, 339, 846
Höfner, S., Jørgensen, U. G., Loidl, R., & Aringer, B. 1998, A&A, 340, 497
Jacob, A. P., Bedding, T. R., Robertson, J. G., & Scholz, M. 2000, MNRAS, 312, 733
Lacy, J. H., Richter, M. J., Greathouse, T. K., Jaffe, D. T., & Zhu, Q. 2002, PASP, 114, 153
Manduca, A. 1979, A&AS, 36, 411
Mennesson, B., et al. 2000, Proc. SPIE, 4006, 481
———. 2002, ApJ, 579, 446
Morgan, N. D., Wasatonic, R., & Guinan, E. F. 1997, Inf. Bull. Variable Stars, 4499, 1
Mozurkewich, D., et al. 1991, AJ, 101, 2207
Perrin, G., Coudé du Foresto, V., Ridgway, S. T., Mennesson, B., Ruilier, C. Mariotii, J.-M., Traub, W. A., & Lacasse, M. G. 1999, A&A, 345, 221
Quirrenbach, A., Mozurkewich, D., Armstrong, J. T., Buscher, D. F., & Hummel, C. A. 1993, ApJ, 406, 215
Rothman, L. S., et al. 1992, J. Quant. Spectrosc. Radiat. Transfer, 48, 469
Schwarzschild, M. 1975, ApJ, 195, 137
Tuthill, P. G., Monnier, J. D., & Danchi, W. C. 1999, in ASP Conf. Proc. 194, Working on the Fringe: Optical and IR Interferometry from Ground and Space, ed. S. Unwin & R. Stachnik (San Francisco: ASP), 188
Weiner, J. 2002, Ph.D. thesis, Univ. California, Berkeley
Weiner, J., Danchi, W. C., Hale, D. D. S., McMahon, J., Townes, C. H., Monnier, J. D., & Tuthill, P. G. 2000, ApJ, 544, 1097
Weiner, J., Hale, D. D. S., & Townes, C. H. 2003, ApJ, 588, 976
White, N. M., & Feierman, B. H. 1987, AJ, 94, 751
Wilson, R. W., Baldwin, J. E., Buscher, D. F., & Warner, P. J. 1992, MNRAS, 257, 369
Wilson, R. W., Dhillon, V. S., & Haniff, C. A. 1997, MNRAS, 291, 819
Woolf, N. J. 1963, Observatory, 83, 260
Ya'ari, A., & Tuchman, Y. 1999, ApJ, 514, L35
Young, J. S., et al. 1999, in IAU Symp. 191, Asymptotic Giant Branch Stars, ed. T. Le Bertre, A. Lebre, & C. Waelkens (San Francisco: ASP), 145